ELSEVIER

Journal of Nuclear Materials 312 (2003) 191–198

journal of nuclear materials

www.elsevier.com/locate/jnucmat

In-pile electrochemical measurements on AISI 316 L(N) IG and EUROFER 97 – I: experimental results

Marc Vankeerberghen *, Rik-Wouter Bosch, Rudi Van Nieuwenhoven

Reactor Materials Research Department, SCK•CEN, TCH Building, Boeretang 200, B-2400 MOL, Belgium

Received 15 July 2002; accepted 15 November 2002

Abstract

In-pile electrochemical measurements were performed in order to investigate the effect of radiation on the electrochemical corrosion behaviour of two materials: reduced activation ferritic–martensitic steel EUROFER 97 and stainless steel AISI 316 L(N) IG. The corrosion potential was continuously monitored during the whole irradiation period. At regular intervals and under various flux levels, polarisation resistance measurements and electrochemical impedance spectroscopy were performed. Polarisation curves were recorded at the end of the reactor cycle. Analysis showed that the corrosion potential increased and the polarisation resistance decreased with the flux level. The impedance data showed two semi-circles in the Nyquist diagram which contracted with increasing flux level. A fit of the impedance data yielded a decrease of solution and polarisation resistances with the flux level. The polarisation curves could be fitted with a standard Butler–Volmer representation after correction for the solution resistance and showed an increase in the corrosion current density with the flux level.

1. Introduction

One of the coolant options for the International Thermonuclear Experimental Reactor (ITER) blanket modules is pressurised water. Hence, it is important to characterise the stress corrosion cracking susceptibility of the candidate structural materials AISI 316 L(N) IG (further referred to as 316 ITER-grade) or EUROFER 97. The composition and heat treatment for both alloys are listed in Table 1. Stress corrosion cracking is an interplay between a material under stress and its environment. It results from the mechanical loading at and the electrochemical behaviour of the material–environment interface. The stress corrosion cracking process is further influenced by radiation. The electrochemical corrosion potential (E_{corr}) of materials in their actual environment is a determining parameter from which their susceptibility to stress corrosion cracking can be inferred. The E_{corr} of a material depends both on the properties of the solution and on the properties of the base material and its protective oxide layer. Ionising radiation (neutrons and gamma's emanating from the burning plasma) will cause radiolysis of the water (leading to the production of hydrogen peroxide) which will strongly affect the E_{corr}. This fact is well known within the fission community where this effect has been studied for many years for the so-called Boiling Water Reactors (BWR) [1]. Whereas no previous (public) studies to investigate the impact of radiation on the E_{corr} of steels in the core of a reactor (in-pile) are known to the authors, the effect of gamma radiation, produced by ^{60}Co sources, has been studied [2] on stainless steel (such as AISI 304) under BWR chemical conditions. It was found that the corrosion potential is significantly affected by the γ-radiation and that radiolysis could account completely for the observed changes. Several publications related to corrosion investigations for nuclear waste disposal showed that γ-radiation will shift the corrosion potential in the positive direction [3–5].

* Corresponding author. Tel.: +32-14 33 34 10; fax: +32-14 32 13 36.

E-mail address: mvankeer@sckcen.be (M. Vankeerberghen).

0022-3115/03/$ - see front matter
PII: S0022-3115(02)01594-5

Table 1
Composition and heat treatment for AISI 316 L(N) IG and EUROFER 97

316 ITER-grade									
Fe	Cr	Ni	Mo	Mn	Si	N	C	Cu	Co
Bal	17.5	12.3	2.3	1.8	0.46	0.06	0.022	0.2	0.17
EUROFER 97									
Fe	C	Si	Mn	P	S	Cr	Mo	Ni	Ta
Bal	0.11	0.05	0.38	<0.005	0.003	8.92	0.0012	0.020	0.15

Normalized at 975 °C for 15 min, cooled to room temperature in air. Tempered at 740 °C for 45 min, cooled to room temperature in air.

The influence of γ-radiation on reference electrodes has been investigated by Taylor and Danielson [6,7]. The effect of intense γ-radiation (comparable to the gamma flux in the core of a BWR), produced by a LINAC, on different reference electrodes and materials was studied by Taylor and revealed significant changes in the corrosion potential [6]. Danielson has used a ^{60}Co source to produce various gamma dose rates [7]. It was shown that there was no measurable effect on the reference electrode potentials at low-dose rates ($< 2.1 \times 10^6$ rad/h). However, one long-lived Ag/AgCl reference electrode failed after a long time of exposure (dose $> 2 \times 10^8$ rad). We believe that, besides radiolysis, the E_{corr} could also be influenced by the direct instantaneous interaction of the neutrons and gamma's with the base material and the passive film (oxide layer). It is known that passive films behave as highly doped and highly defective n-type semiconductors and, in analogy to the well-known effects of light on semiconductors, the effect of radiation on oxidised metals is designated as the radiation photo effect. When the radiation is switched off, the photo effect also decays rather quickly [8]. It has been demonstrated in the laboratory [9–11] that UV light has a significant impact on pitting corrosion and this has been attributed to the generation of mobile charge carriers (electron–hole) within the film. Besides the direct effect on the passive layer, gamma and neutron interactions with the base material can lead to free electron producing reactions which could also alter the E_{corr}. Gamma interactions could lead to electron emission from the base material through the Compton effect, while neutrons could lead to capture gamma rays which in turn may generate free electrons due to the Compton effect. Therefore, it is important to investigate whether the E_{corr} is not only changed indirectly by radiolysis but also by more direct processes as the ones discussed above.

As such, it was important to investigate the electrochemical behaviour of the two candidate materials for the first wall, namely 316 ITER-grade and EUROFER 97. The electrochemical behaviour of these two candidate materials was examined in-pile in the BR2 materials testing reactor in an experiment called COFUMA (COrrosion of FUsion MAterials). The electrochemical characterisation involved the continuous recording of the corrosion potential (E_c) against an in-pile platinum reference electrode (IPRE) and an out-of-flux platinum reference electrode (OPRE) and, at regular intervals, the measurement of the polarisation resistance (R_p) and the execution of electrochemical impedance spectroscopy (EIS). Polarisation curves were recorded at the end of the reactor cycle.

The aim of the COFUMA experiment was to measure the electrochemical behaviour of fusion materials in-pile so that the influence of irradiation on electrochemical parameters could be unravelled. Hence, the main objectives of the experiment were to

(1) demonstrate the in-pile execution of electrochemical measurements: corrosion potential, polarisation resistance, polarisation curve and impedance plot,
(2) measure the shift in electrochemical parameters due to radiation using a local, in-pile platinum electrode as a reference electrode, and
(3) measure the radiation-induced shift in electrode potential of the local, in-pile platinum electrode against an out-of-pile platinum reference electrode.

This paper shows that electrochemical measurements could be performed successfully in the core of the BR2 materials testing reactor, and a detailed discussion on the obtained results is presented.

2. Experimental

2.1. Experimental set-up

The *in-pile section* (IPS) is made of one single stainless steel tube to which electrodes and sensors are fixed. In the test section there are seven electrodes: one IPRE, three specimens (surface area 6.26 cm^2) made of 316 ITER-grade material and three specimens (surface area 6.26 cm^2) made of EUROFER 97 material. An out-of-core platinum reference electrode (OPRE) is fixed about

3 m higher in the IPS. Seven detectors are mounted: three thermocouples (TC), two rhodium self-powered neutron detectors (Rh-SPND) and two gamma-thermometers (GT). The neutron flux in the test section is varied by moving the rig step-wise into or out of a thimble tube. The *out-of-pile section* (OPS) consists of instrumentation related equipment. Indeed, the electrode and sensors signals are fed to a general data acquisition system or an electrochemical analysis system.

2.2. Electrochemical measurements

The electrochemical measurements were performed in a standard three-cell electrode arrangement. The in-pile reference electrode (IPRE) is located in the centre of the test section, assuring symmetry. The 316 stainless steel structure of the rig is used as counter electrode. The specimens are located around the IPRE and are electrically insulated from the rig structure by ceramic pins. One mineral-insulated and shielded cable was connected to each of the specimen and the IPRE. All the measurement cables were brought to a terminal block to which the measurement systems were branched. Open circuit potentials were measured at one minute intervals by an Agilent® data acquisition system. Specific electrochemical measurements were controlled by a multiplexed GAMRY® potentiostat system. At regular intervals the latter system performed corrosion potential (E_{corr}), polarisation resistance (R_p) and EIS measurements. At the end of the testing period polarisation curves were recorded. The polarisation resistance was determined with the linear polarization resistance (LPR) technique. The potential was scanned from −10 to +10 mV against the open circuit potential with a scan rate of 0.5 mV/s and a sampling time of 2 s. EIS was performed from 1000 to 0.01 Hz with a perturbation amplitude of 10 mV RMS around the open circuit potential. Polarisation curves were measured from −500 to +2000 mV against the open circuit potential with a scan rate of 600 mV/h (ASTM G 5-94) and a sampling time of 10 s. The potential of the OPRE has been measured continuously against the potential of the IPRE. This allowed the corrosion potentials of the six specimens to be converted from measurements against IPRE to measurements versus OPRE using $E_{corr}^{OPRE} = E_{corr}^{IPRE} - E_{OPRE}^{IPRE}$.

2.3. Neutron and gamma flux measurements

The rig contains two self-powered neutron detectors (SPNDs) to measure the instantaneous thermal neutron flux and two gamma thermometers (GTs) to measure the instantaneous gamma flux. The mid-plane of the SPNDs/GTs lies 132 mm above the mid-plane of the test section. Hence, the thermal neutron (gamma) flux, as measured by the SPNDs (GTs), has been corrected to yield the thermal neutron (gamma) flux at the axial location of the specimens using measured axial flux profiles from previous reactor experiments (Fig. 1). Furthermore the SPNDs (GTs) are also not located at the angular positions of the specimens. Hence, the thermal neutron (gamma) flux, as measured by the SPNDs (GTs), has also been converted to yield the thermal neutron (gamma) flux at the angular positions of the specimens.

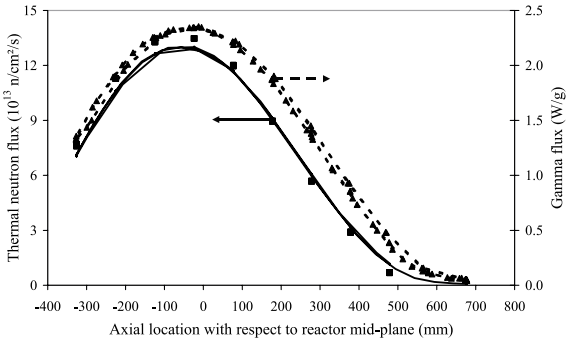

Fig. 1. Profile measurement performed in channel L180 of the BR2 materials testing reactor during the DOLMEN reactor experiment, cycle 2/2001. The continuous line corresponds to thermal neutron flux measurements with a 21 cm long Co SPND. The squares correspond to thermal neutron flux measurements with a 5 cm long Ag/Rh SPND. The dashed line and triangles correspond to measurements taken with a gamma thermometer.

3. Results and discussion

3.1. Corrosion potential

Multiple corrosion potential (E_{corr}) measurements have been performed before, during and after reactor cycles 5A and 5B. The spreading on the corrosion potential measurements was relatively small and the inter-specimen variation of the corrosion potential was relatively low. Fig. 2 shows the variation of the corrosion potential and the temperature versus the thermal neutron flux, averaged by specimen/material and rig position. Differences in electrochemical behaviour can in most cases be related to the difference in composition of both alloys. EUROFER 97 contains not more than 9% chromium, which is not sufficient to passivate the whole surface. 316 ITER-grade is a fully austenitic stainless steel and will be completely passivated under the given experimental conditions. The following conclusions can be drawn:

- The corrosion potential is lower for the EUROFER 97 than for the 316 ITER-grade material, which can be related to the fact that EUROFER 97 is only partly passivated.

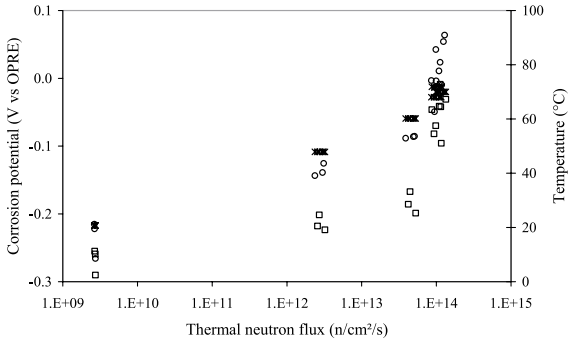

Fig. 2. Corrosion potential as measured against the OPRE and temperature as a function of the thermal neutron flux. Averaging by specimen/material and rig position. Circles represent 316 ITER-grade, squares EUROFER 97 and stars temperature.

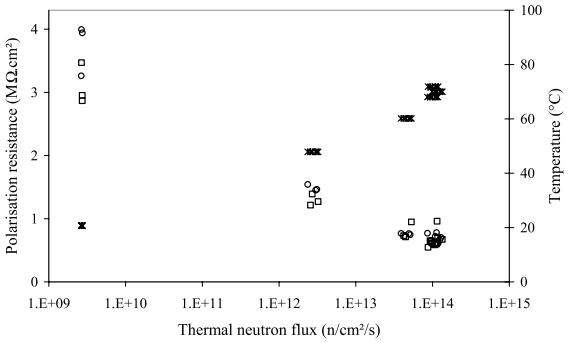

Fig. 3. Polarisation resistance and temperature as a function of the thermal neutron flux. Averaging by specimen/material and rig position. Circles represent 316 ITER-grade, squares EUROFER 97 and stars temperature.

- The corrosion potential increases with the neutron flux for both materials. However, the corrosion potential seems to be more determined by the temperature than by the thermal neutron flux, as can bee seen from the trend in Fig. 2.
- The sensitivity of the corrosion potential to the temperature/neutron flux is higher for the 316 ITER-grade than for the EUROFER 97 material. This can be related to the difference in polarization behaviour of both materials. EUROFER 97 will still show some active corrosion and is therefore less polarisable than ITER 316, i.e. the polarisation curve around the corrosion potential is less steep for EUROFER 97 than for 316 ITER-grade.

3.2. Polarisation resistance

Multiple polarisation resistance (R_p) measurements have been performed before, during and after reactor cycle 5A and 5B. The spreading on the polarisation resistance data was larger than on the corrosion potential data. Inter-specimen variation of the polarisation resistance was relatively low. Fig. 3 shows the variation of the polarisation resistance and the temperature versus the thermal neutron flux, averaged by specimen/material and rig position. The following conclusions can be drawn:

- The polarisation resistance decreases with the thermal neutron flux and seems to be fully determined by the thermal neutron flux. This confirms the idea that a neutron flux will lower the polarisation resistance (or increase the corrosion rate) by the combined interaction of the production of oxidants by radiolysis, an increasing temperature due to gamma-heating and possibly a direct flux effect.
- The sensitivity of the polarisation resistance to the neutron flux is higher for the 316 ITER-grade than for the EUROFER 97 material. Again this can be related to the difference in electrochemical behaviour i.e. 316 ITER-grade is fully passivated and EUROFER 97 is not.
- The polarisation resistance is lower for the EUROFER 97 than for the 316 ITER-grade material at low thermal neutron flux, which can be related to the incomplete coverage of the EUROFER 97 material by an oxide layer.
- With increasing flux level the polarisation resistance of both materials is getting similar as shown in Fig. 3. This might be caused by the fact that the anodic reaction could be increasingly dominated by redox reactions involving radiolysis products than by anodic dissolution. Then the electrochemical behaviour would become independent of the electrode material and similar for both alloys.

3.3. Electrochemical impedance

Multiple EIS measurements have been performed before, during and after reactor cycle 5A and 5B. The impedance data show two semi-circles in the Nyquist diagram (Fig. 4). The semi-circles contract with an increase in the flux level. The impedance measurements can be fit to the equivalent circuit shown in Fig. 5 [12]. An equivalent circuit can be used to fit impedance data over the whole frequency range of interest which, for electrochemical systems, is in the range 100 kHz to 1 mHz. Here, the fit results have been calculated for experimental data over the frequency range 1000–0.01 Hz. This frequency range was sufficient to obtain the electrochemical parameters as can be seen from the goodness of the fit in Fig. 5. The resistance R_1 is related to the solution resistance between the reference electrode and the working electrode. The capacitor C_1 is related to the capacitance of the solution, which can be observed in systems with a very high solution resistance. Typical

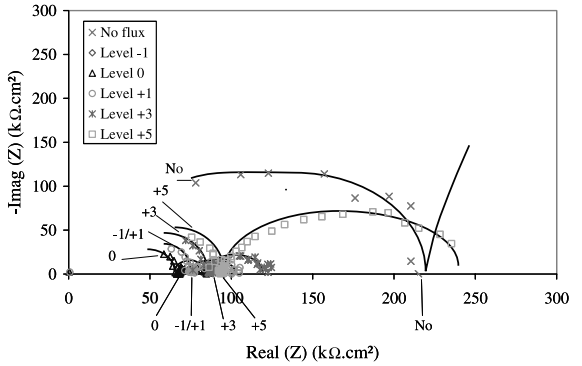

Fig. 4. Nyquist diagram for selected electrochemical impedance measurements on specimen 1. Notice the two semi-circles nature (hand-drawn). Rig levels 1, 0, +1, +3 and +5 indicate that the test section is, respectively, −100, 0, +100, +300 and +500 mm from the reactor mid-plane (highest flux).

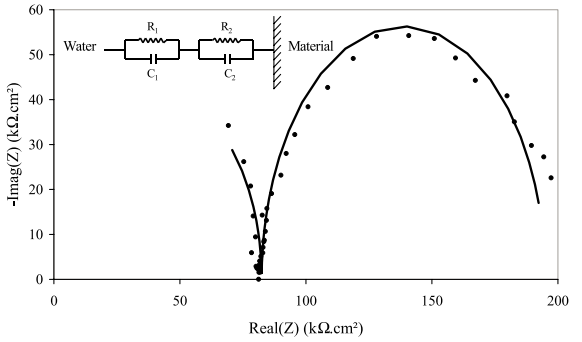

Fig. 5. Typical curve-fitting result in the Nyquist diagram. The equivalent circuit used for fitting the impedance measurements is shown at the top left.

values are in the order of 10^{-10} F cm^{-2} which is close to the values measured. The resistance R_2 is related to the charge transfer reaction at the working electrode and the capacitor C_2 is related to the capacitance of the electrochemical double layer. The two RC-cell impedance Z be expressed as

$$Z = \frac{\frac{1}{R_1} - j\omega C_1}{\frac{1}{R_1^2} + \varpi^2 C_1^2} + \frac{\frac{1}{R_2} - j\omega C_2}{\frac{1}{R_2^2} + \varpi^2 C_2^2}. \quad (1)$$

The values of the parameters R_1, R_2, C_1 and C_2 have been obtained for all impedance measurements by curve-fitting the experimental data with the expression for the real or the imaginary part of the impedance Z. An example of a fitting result is given in Fig. 5.

- R_1 – Very little inter-specimen and inter-material variation was noted. Fig. 6 shows a summary of the results for R_1 as a function of the thermal neutron flux. The results are averaged by specimen/material and rig position. R_1 strongly decreases with the neutron flux. There is no difference between the 316 ITER-grade and EUROFER 97 material.
- R_2 – Very little inter-specimen variation was noted. Fig. 7 shows a summary of the results for R_2 as a function of the thermal neutron flux. The results are averaged by specimen/material and rig position. R_2 strongly decreases with the thermal neutron flux. The R_2 values are generally higher for the 316 ITER-grade than for the EUROFER 97 material, especially at low flux.
- C_1 – Some inter-specimen variation is noted. The results, averaged by specimen/material and rig position, showed that C_1 values are generally higher for the 316 ITER-grade than for the EUROFER 97 material. No immediate influence of the thermal flux on C_1 was apparent.
- C_2 – Very little inter-specimen variation was noted. The results, averaged by specimen/material and rig position showed that C_2 values were generally higher for the 316 ITER-grade than for the EUROFER 97

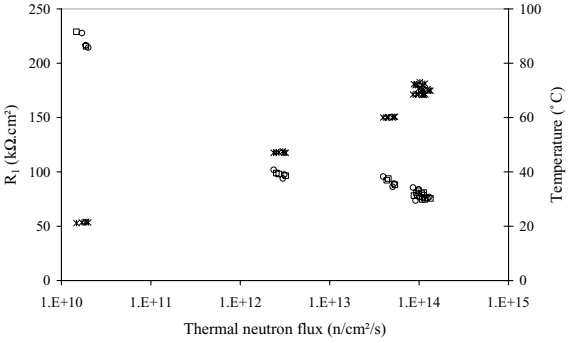

Fig. 6. EIS fitting results – R_1 parameter and averaged temperature as a function of the thermal neutron flux. Averaging by specimen/material and rig position. Circles represent 316 ITER-grade, squares EUROFER 97 and stars temperature.

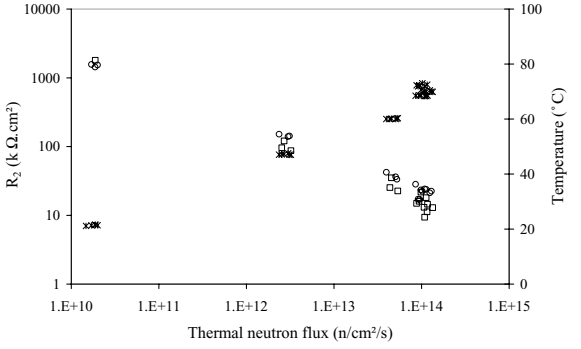

Fig. 7. EIS fitting results – R_2 parameter and averaged temperature as a function of the thermal neutron flux. Averaging by specimen/material and rig position. Circles represent 316 ITER-grade, squares EUROFER 97 and stars temperature.

material. C_2 seemed to increase with the thermal neutron flux.

The following conclusions can be drawn:

- R_1 decreases strongly with the thermal neutron flux and is independent of the material. Hence, we assume that R_1 is mainly influenced by radiolysis which alters the water chemistry.
- R_2 decreases strongly with the thermal neutron flux, is slightly higher for the 316 ITER-grade material and decreases more sharply with the thermal neutron flux for the 316 ITER-grade material.
- C_1 does not change with the thermal neutron flux and is larger for the 316 ITER-grade material.
- C_2 increases slightly with the thermal neutron flux and is slightly higher for the 316 ITER material.

Summarizing, the Nyquist diagram shows two semicircles and could be fit by an equivalent circuit of two RC cells in series. The first RC cell is related to processes in the water and the second one to the charge transfer reaction and the electrochemical double layer.

Notice that the polarisation resistance obtained by EIS (R_2) is a factor of ten lower than the polarisation resistance obtained from the LPR measurements. This is the result of the high resistivity of the environment [13] and henceforth the EIS values will be used.

3.4. Polarisation curves

Six polarisation curves have been recorded during reactor cycle 5B, one on each specimen in the COFUMA rig. Fig. 8 shows an example of a recorded polarisation curve. It is believed that the large ohmic drop in the solution affects the measurements and even has an overriding effect. A correction for this ohmic drop can be made in the following way [14]. The standard form for a Butler–Volmer type representation of the charge transfer reaction is

$$i = i_{\mathrm{corr}}\left(\mathrm{e}^{\frac{E-E_{\mathrm{corr}}}{\beta_{\mathrm{a}}}} - \mathrm{e}^{\frac{E-E_{\mathrm{corr}}}{\beta_{\mathrm{c}}}}\right), \tag{2}$$

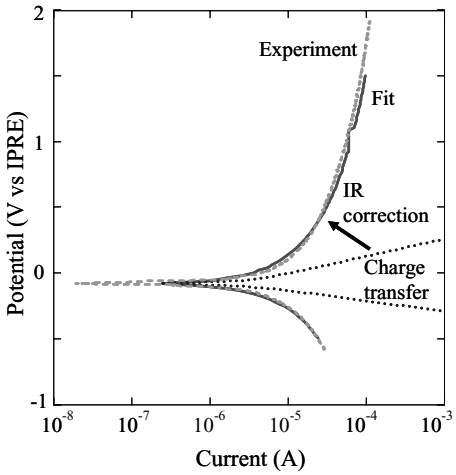

Fig. 8. Fit to the polarisation curve for specimen 6. The dashed line represent the measurement, the continuous line the 'ohmic drop'-corrected calculation and the dotted line the bare charge transfer reaction kinetics. Specimen area is 6.26 cm^2.

where E is the electrode potential, E_{corr} the corrosion potential, i the charge transfer current density, i_{corr} the corrosion current density and β_{a} and β_{c} the Tafel constants for the anodic and cathodic branch, respectively. This expression can be modified to take the ohmic drop into account by changing it into

$$i = i_{\mathrm{corr}}\left(\mathrm{e}^{\frac{E-E_{\mathrm{corr}}-iR_{\mathrm{ohm}}}{\beta_{\mathrm{a}}}} - \mathrm{e}^{-\frac{E-E_{\mathrm{corr}}-iR_{\mathrm{ohm}}}{\beta_{\mathrm{c}}}}\right), \tag{3}$$

where R_{ohm} is the ohmic resistance. The corrosion current density i_{corr} is related to the polarisation resistance R_{p} as follows

$$I_{\mathrm{corr}} = \frac{\beta_{\mathrm{a}}\beta_{\mathrm{c}}}{2.303(\beta_{\mathrm{a}}+\beta_{\mathrm{c}})R_{\mathrm{p}}}. \tag{4}$$

Estimates for the values of R_{ohm} and R_{p} have been obtained from the EIS measurements and are listed in Table 2. All recorded polarisation curves have subsequently been curve-fit to obtain the Tafel constants β_{a}

Table 2
Estimates of the parameters used in the Butler–Volmer expression for the charge transfer reaction

Specimen	Rig level	Material	R_{ohm} ($=R_1$) ($\Omega\,\mathrm{cm}^2$)	R_{p} ($=R_2$) ($\Omega\,\mathrm{cm}^2$)	E_{corr} (V)	β_{a} (V)	β_{c} (V)	i_{corr} ($\mu\mathrm{A/cm}^2$)
3	−1	316 ITER	84028	23475	0.025	0.0408	0.0475	2.54
4	−1	EUR 97	81029	18073	−0.078	0.0675	0.0461	4.12
1	+1	316 ITER	76491	24189	0.037	0.0276	0.0467	1.95
2	+1	EUR 97	80604	15976	−0.072	0.0489	0.0476	4.10
5	+3	316 ITER	89599	33072	0.050	0.0331	0.0471	1.60
6	+3	EUR 97	88454	23337	−0.082	0.0569	0.0362	2.58

Rig levels −1, +1 and +3 indicate that the test section is, respectively, −100, +100 and +300 mm from the reactor mid-plane (highest flux).

and β_c. The values for E_{corr} listed in Table 2 are read off from the data records of the polarisation curves. The final results are listed in Table 2 and in Fig. 8. In these figures the dotted line corresponds to the pure charge transfer reaction, the continuous line to the charge transfer reaction after correction for the ohmic drop and the dashed line to the measured polarisation behaviour. Good agreement between the measurements and the 'ohmic drop'-corrected calculations can be seen in all cases.

Table 2 lists the estimates of the parameters E_{corr}, i_{corr}, β_a and β_c used in the Butler–Volmer expression for the charge transfer reaction. The following conclusions can be drawn (note that −1 is the highest flux and +3 the lowest flux level):

- The corrosion current density i_{corr} increases with the flux and is larger for the EUROFER 97 than for the 316 ITER-grade material.
- The anodic Tafel parameter β_a is larger for the EUROFER 97 than for the 316 ITER-grade material and might increase slightly with the flux.
- The cathodic Tafel parameter β_c seems to increase with the flux for EUROFER 97 and is slightly higher for the 316 ITER-grade than for the EUROFER 97 material.

Summarizing, using an 'ohmic drop' correction all polarisation curves could be fitted by a Butler–Volmer expression. The 'ohmic drop' and polarisation resistances of the impedance measurements were used during the fitting process, which yielded the anodic and cathodic Tafel parameters and the corrosion current.

3.5. Results obtained during start-up

During the two reactor start-ups the corrosion potential of the six specimens and the potential of the OPRE were continuously monitored against the IPRE. The results of the measurements are shown in Fig. 9 for reactor cycle 5A and 5B. There is a sharp increase in corrosion potential (against OPRE) just after the reactor start-up. Might this be an indication of a direct flux effect?

3.6. Results obtained during reverse and scram

The objective of the reverse and scram was to identify a sudden change in corrosion potential after a reactor stop. During the reactor stop the corrosion potential of the six specimens and the potential of the OPRE were continuously monitored against the IPRE. The data acquisition speed was increased to one measurement per second. The results of the measurements are shown in Fig. 10. There is no sharp change in the corrosion potential (against OPRE) just after the reverse or scram.

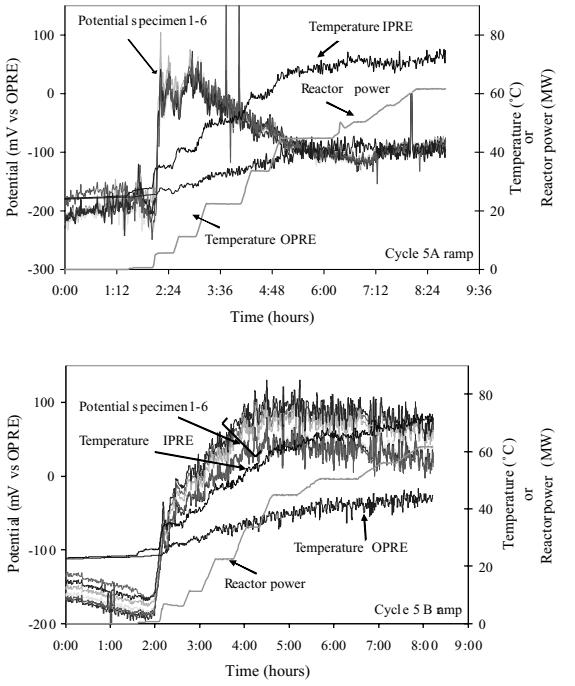

Fig. 9. The evolution of the corrosion potential, the reactor power, and the OPRE and IPRE temperature during reactor start-up for cycle 5A and 5B.

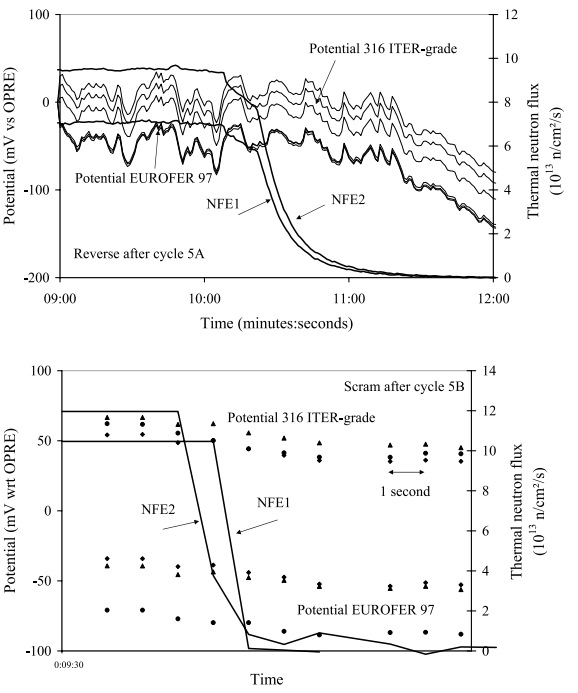

Fig. 10. The evolution of the corrosion potential (measured against the OPRE) of the six specimens during a reactor reverse at the end of reactor cycle 5A and a scram at the end of reactor cycle 5B.

Hence, a direct effect of radiation on the corrosion potential does not seem to be observed.

4. Conclusion

In-pile electrochemical measurements were successfully performed in the BR2 materials testing reactor at SCK•CEN. The results showed that the corrosion potential increased and the polarisation resistance decreased with the flux level. The impedance data showed two semi-circles in the Nyquist diagram which contracted with increasing flux level. The two semi-circles could be fit by an equivalent circuit of two RC cells in series. The first RC cell is related to processes in the water and the second one to the charge transfer reaction and the electrochemical double layer. A fit of the impedance data yielded a decrease of the solution and polarisation resistances with the flux level. The polarisation curves could be fitted with a standard Butler–Volmer representation after correction for the solution resistance and showed an increase in the corrosion current density with the flux level.

Acknowledgements

The partial sponsoring of this work by the Underlying Technology Task of the European Fusion Technology Programme under Association Contract FU05-CT-2001-00322 is greatly acknowledged. Sincere thanks also go to the technical staff at SCK•CEN for without their dedication these measurements would not have been possible.

References

[1] P. Scott, J. Nucl. Mater. 211 (1994) 101.
[2] N. Saito, H. Sakamoto, E. Kikuchi, J. Kuniya, S. Suzuki, Corrosion 53 (1997) 537.
[3] R.S. Glass, G.E. Overturf, R.A. Van Konynenburg, R.D. McCright, Corros. Sci. 26 (1986) 577.
[4] Y.J. Kim, R.A. Oriani, Corrosion 43 (1987) 85.
[5] G.P. Marsh, K.J. Taylor, G. Bryan, S.E. Worthington, Corros. Sci. 26 (1986) 971.
[6] D.F. Taylor, Corrosion 47 (1991) 115.
[7] M.G. Danielson, Corrosion 51 (1995) 450.
[8] A.V. Bjalobzeskii, Korrosion durch Strahlung, EDV-Nr. 7614376, Printed in German Democratic Republic, 1970.
[9] D.D. Macdonald, E. Sikora, M.W. Balmas, R.C. Alkire, Corros. Sci. 38 (1) (1996) 97.
[10] C.B. Breslin, D.D. Macdonald, J. Sikora, E. Sikora, Electrochim. Acta 42 (1) (1997) 127.
[11] C.B. Breslin, D.D. Macdonald, J. Sikora, E. Sikora, Electrochim. Acta 42 (1) (1997) 137.
[12] R. Cottis, S. Turgoose, in: B.C. Syrett (Ed.), Electrochemical Impedance and Noise, NACE – Corrosion Testing Made Easy, 1999, p. 29 [ISBN 1-57590-093-9].
[13] Linear polarization resistance, Materials Performance, May 2002, p. 10.
[14] N.G. Thompson, J.H. Payer, in: B.C. Syrett (Ed.), DC Electrochemical Test Methods, NACE – Corrosion Testing Made Easy, 1998, p. 87 [ISBN 1-877914-63-0].